TRANSPORT IN SEMICONDUCTORS, DYNAMICS OF CARRIERS IN MACROSCOPIC AND MESOSCOPIC SYSTEMS

To understand the transport phenomena in semiconductor crystals one needs to know a multitude of interrelated concepts, including the electronic band structure of semiconductors, crystal lattice dynamics, and electron–phonon interaction. This article is an overview of these and several other closely related topics.

The transport of electrons inside a semiconductor crystal has very complicated dynamics. To start, in one cubic centimeter of a typical crystal there are approximately 10^{23} electrons interacting with an equally large number of nuclei. The atoms of the crystal are attached to one another by covalent bonds (electrons that are shared between neighboring atoms), which can be considered as "springs" connecting heavy ions. These ions are vibrating around an equilibrium position. These vibrations, which exist at any temperature (and increase as the temperature of the crystal is raised) are described by small packets of thermal (or vibrational) energy referred to as *phonons*. Electrons, in their movement inside the crystal, are scattered by these phonons. *Scattering* is a generic term used for collisions between carriers and the obstacles that the carriers might face. These collisions impede the motion of electrons. The strength of the scattering (the intensity of the collision) is dependent on the energy and momentum of the electrons as well as the energy and momentum of phonons.

To describe the transport phenomenon we do the following in successive sections:

1. Approximate the behavior of the ensemble of real electrons in real crystals with a realistic number of differential equations that can be solved analytically or numerically.
2. Discuss the time frames within which the scattering of carriers take place, and limit the study of transport to time frames longer than several limiting time intervals.
3. Determine the momentum dependence of the energy of carriers in the crystal. It turns out that the parabolic relationship between the energy and momentum ($E = p^2/2m$) for free electrons is altered when electrons are inside the crystal and experience the internal forces within the crystal.
4. Assign an effective mass to electrons such that the nonparabolic energy–momentum relationship for electrons can be accounted for by a simple replacement of the free-carriers mass with effective mass. The effective mass is connected with the energy band structure.
5. Study the dynamics of the crystal lattice vibrations, and discuss various modes of the resulting phonons. One also needs the energy and momentum dependence, as well as the range of frequencies, of these phonons. This study is needed before any interaction of electrons and phonons can be investigated.
6. Establish a rule of interaction between the scatterers and electrons, referred to as Fermi's "golden rule."
7. Define certain characteristic times (referred to as relaxation times) that approximate the process of return of the ensemble of electrons to its equilibrium state. For example, when the energy (or momentum) of the ensemble of electrons is disturbed by an applied force (electric or magnetic), the energy attained by electrons must somehow be dissipated and transferred to the crystal. The relaxation times are parameters that characterize this dissipation and the return of the ensemble to its equilibrium state.
8. Calculate the rate by which carriers are scattered by the various scatterers, which include phonons, impurities, and others. Scattering rates are computed from the scattering potentials and are approximated by power-law energy-dependences. A complete derivation of scattering rates due to ionized impurities and certain selected phonons scattering rates is given.
9. Formulate a simple model for the conductivity of carriers in terms of the transport of electrons within the crystal. This conductivity model is related to the *mobility* of carriers.
10. In the last Section of this article we introduce several concepts related to the transport in mesoscopic devices (also referred to as nanostructures or nanodevices).

This article, which is the first of a two-article series, ends with the discussion of the conductivity model. All the materials presented in this article are groundwork for a second article entitled: "Semiconductor Boltzmann Transport Equation in Macroscopic and Quantum-Confined Systems.

APPROXIMATING THE DYNAMICS OF REAL ELECTRONS IN REAL CRYSTALS

Setting aside the effects of imperfections in the crystals, and assuming a perfect crystal, the *Hamiltonian* (the mathematical operator associated with the total energy) can be written as (1)

$$\mathcal{H} = \sum_i \frac{p_i^2}{2m_i} + \sum_j \frac{P_j^2}{2M_j} + \frac{1}{2}\sum_{j\neq j'} \frac{Z_j Z_{j'} e^2}{\|R_j - R_{j'}\|} - \sum_{j,i} \frac{Z_j e^2}{\|r_i - R_j\|} + \frac{1}{2}\sum_{i\neq j} \frac{e^2}{\|r_i - r_j\|} \tag{1}$$

In this expression r_i denotes the position of the ith electron, R_j is the position of the jth nucleus, Z_j is the atomic number of the jth nucleus, p_i and P_j are the momentum operators of the electrons and nuclei, respectively, and $-e$ is the electronic charge. The masses of the electrons and nuclei are denoted as m_i and M_j, respectively. Each term in the Hamiltonian expressed in Eq. (1) describes a different contribution to the total energy. The first two terms, $S_i\, p_i^2/2m_i$ and $S_j P_j^2/2M_j$, are the kinetic energies of electrons and the nuclei, respectively. The third term, ½ $S_{j\neq j}$, $Z_j Z_j$, $e^2/\|R_j - R_j\|$, is the energy associated with the

J. Webster (ed.), *Wiley Encyclopedia of Electrical and Electronics Engineering*. Copyright © 2007 John Wiley & Sons, Inc.

interactions among the nuclei; the fourth term, $S_{j,i} Z_j e^2/\|r_i - R_j\|$, is that associated with the interactions between the electrons and the nuclei. The last term, $\frac{1}{2} S_{i\neq j} e^2/\|r_i - r_j\|$ represents the interactions among the electrons. Considering the fact that there are approximately 10^{23} electrons in each cubic centimeter of the crystal, and an equally large number of nuclei, the task of solving the system of coupled equations described in the above *many-particle Hamiltonian* is formidable. It turns out that solving even one of these equations is equally nontrivial.

To proceed, one needs a large number of approximations. The first approximation is to separate the electrons into two groups: *valence electrons* and *core electrons*. The core electrons, which are mostly localized around the nuclei, can be lumped together with the nuclei to form the *ion core*. The electrons in the incompletely filled shells (3*s* and 3*p* electrons in silicon) are the valence electrons. This approximation is well justified in that the electrical and electronic properties of semiconductors (and other materials for that matter) are mostly due to the valence electrons.

The next approximation invoked is the *Born–Oppenheimer* or *adiabatic approximation,* in which it is assumed that so far as the valence electrons are concerned, the ion cores are essentially stationary. The typical frequency of ionic vibration in crystals is about 10^{13} Hz, whereas the typical response time (see the following section) of electrons (in a semiconductor with 1 eV bandgap) corresponds to a frequency of about 10^{15} Hz. As a result, electrons can respond to ionic motions almost instantly, while the ions cannot follow the motion of electrons. So, from the point of view of ions, the motion of electrons creates only a *time-averaged adiabatic potential*. With the Born–Oppenheimer approximation the Hamiltonian in Eq. (1) can be written as

$$\mathscr{H} = \mathscr{H}_{\text{ions}}(R_j) + \mathscr{H}_{\text{e-ion}}(r_i, \delta R_j) + \mathscr{H}_{\text{e}}(r_i, R_{j0}) \tag{2}$$

In Eq. (2), the term $H_{\text{ions}}(R_j)$ is the Hamiltonian describing the ionic motion under the influence of the ionic potential plus the time-averaged adiabatic potential. This ionic motion is responsible for creating several branches of phonons, which act as scatterers of electrons, and is discussed in detail in the section "Phonons and Lattice Dynamics." The second term in Eq. (2), $H_{\text{e–ion}}(r_i, dR_j)$, represents the electron energy due to the interaction (scattering) of electrons with displacement of ions (dR_j), which is the well-known *electron–phonon interaction,* and is discussed in three sections thereafter. The last term $H_e(r_i, R_{j0})$ in Eq. (2) describes the interaction of electrons with the ions frozen in their equilibrium position R_{j0}, and can be written as

$$\mathscr{H}_{\text{e}}(r_i, R_{j0}) = \sum_i \frac{p_i^2}{2m_i} + \frac{1}{2}\sum_{i\neq i'} \frac{e^2}{\|r_i - r_{i'}\|} - \sum_{j,i} \frac{Z_j e^2}{\|r_i - R_{j0}\|} \tag{3}$$

The above Hamiltonian, although significantly simpler than the Hamiltonian given by Eq. (1), still involves matrices of dimension 10^{23}. To make solution possible, a drastic approximation known as *mean-field approximation* is made, in which it is assumed that every electron experiences the *same average potential* $V(r)$. With this rather oversimplifying approximation, the Schrödinger equation describing the motion of each electron will be given by

$$\mathscr{H}_{1e}\psi_n(r) = \left(\frac{p^2}{2m} + V(r)\right)\psi_n(r) = E_n\psi_n(r) \tag{4}$$

Here H_{1e}, $y_n(r)$, and E_n are *one-electron* Hamiltonian, the eigenfunction, and the energy of an electron in an eigenstate, respectively. Each eigenstate, denoted by n, can accommodate two electrons of opposite spin.

Only for a few simple potentials $V(r)$ can the Schrödinger equation be solved analytically. Three such closed-form solutions for three prototype problems—namely, the harmonic oscillator (crystal vibrations), an electron in a potential well (quantum wells), and an electron in a central force (hydrogen atom)—can be found in any quantum mechanics text. [See for example White (2) or Yariv (3).]

TIME SCALES IN THE TRANSPORT OF ELECTRONS IN SEMICONDUCTORS

The motion of electrons in a semiconductor is not collision-free. Electrons, when subjected to a force (electric or magnetic, internal or external), undergo a series of collisions with a number of scattering particles. The collisions are present even when there is no applied field. In fact, it is these collisions that provide the mechanism of exchange of energy and momentum with the lattice and other carriers. There are collisions between the carriers (electrons or holes), which randomize the energy and momentum of the *ensemble* of carriers. Then there are elastic collisions between the carriers and impurities or acoustic phonons, and finally there are inelastic collisions between the carriers and the lattice vibrations in the form of optical phonons. Which of these scattering mechanisms become dominant depends on the semiconductor material, the strength of the applied field, the temperature, the level of doping, and several other parameters. When an external force is applied, the electrons, while being accelerated, exchange their energy and/or momentum with other particles (meaning other electrons, or ionized and neutral impurities, acoustic or optical phonons, etc.). This exchange, depending on the type of scattering mechanism involved, relaxes the energy, or the momentum, or both the energy and the momentum, of the ensemble of electrons to their equilibrium states, provided that the external force has not disturbed the carriers far from equilibrium.

There are finite time intervals involved in all of these collisions and relaxations to equilibrium. In general there are four time scales involved: (1) τ_C, the average time *duration* of the collision, (2) τ_F, the average time *between* two consecutive collisions, which is also known as the *mean free time*, (3) τ_R, the characteristics time associated with the return of a disturbed electron distribution to its equilibrium distribution, also known as the *relaxation time* (depending on the collision mechanism involved, it can be either an *energy* or a *momentum* relaxation time), and (4) the hydrodynamic time τ_H, the characteristic time associated with the return of a nonuniform (nonhomogeneous) distribution of electrons to its uniform distribution. The collision time τ_C is extremely short, and is the least important of all. The

mean free time τ_F is usually much longer than τ_C, except under high electric fields, where the mean free time and the collision time are comparable and one encounters several new transport effects, such as hot-electron transport and the Stark effect. The quantities that are characterized by the relaxation time τ_R are momentum (momentum relaxation time, τ_m), and energy (energy relaxation time τ_e). Relaxation in momentum returns the system to a *local* equilibrium, whereas relaxation in energy returns the system to an *ensemble* equilibrium. These relaxation times are still longer than the mean free time τ_F. When there is a carrier concentration gradient (as in external injection of carriers into a crystal), the establishment of a uniform distribution, or a nonequilibrium steady state, takes place on time scales comparable to the hydrodynamic time τ_H, which is the longest of all four time scales. It is only on the scale of τ_H that the process is truly *ergodic*-that is, such that time averages are equal to ensemble, or distribution, averages, which are the important averages. In summary, the time scales in transport of electrons in semiconductors can be written as (4)

$$\tau_C < \tau_F < \tau_R < \tau_H \tag{5}$$

Studying transport phenomena in semiconductors involves investigating the transient behavior of carriers and the evolution of their distribution with time. In fact, the Boltzmann transport equation, described in a separate article immediately following, describes the temporal evolution of a distribution function that is defined for carriers in a space referred to as *phase space*, consisting of position, momentum, and time. The validity of the Boltzmann equation becomes seriously questionable when the time scales of interest are shorter than the time scales described above. In fact, it is only within the time scales comparable to the hydrodynamic time τ_H that the transport of carriers in semiconductors can be described by the Boltzmann transport equation.

ELECTRONIC BAND STRUCTURE

The energy–momentum relationship $E(k)$ for a free electron (an electron that is free from any internal scattering forces within a crystal) is parabolic, and the electron is allowed to attain a continuous range of energies proportional to square of the momentum k. Within the crystal, and when subjected to internal scattering forces of the lattice, the $E(k)$ relationship loses its parabolicity and acquires discontinuities in the form of forbidden energy gaps. The formation of such forbidden gap (called a *bandgap*) is the basis of many electrical and optical properties of all semiconductors.

Furthermore, the $E(k)$ relationship of electrons provides for yet another important simplification useful for the description of transport within the crystal, which is the *effective-mass approximation* for the carriers. In this approximation, the effect of the crystal lattice potential on the transport is included by using an effective mass, and thus transport of carriers under the influence of an external field can be described easily. To obtain the $E(k)$ relationship, one needs to solve the one-electron time-dependent

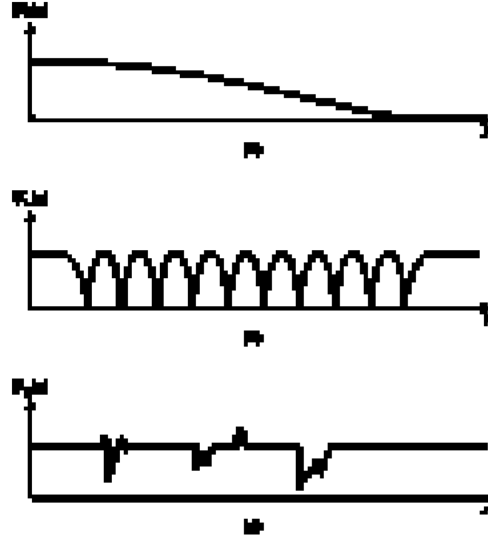

Figure 1. A schematic plot of the three components of the potential energy U of electrons: $U = U_E + U_L + U_S$. (a) Macroscopic potential U_E; (b) periodic lattice potential U_L, and (c) scattering potential, U_S. After Datta (5); reprinted with permission.

Schrödinger equation given by

$$-\frac{\hbar^2}{2m_0}\nabla^2\psi_0(\boldsymbol{r},t) + U(\boldsymbol{r},t)\psi_0(\boldsymbol{r},t) = -\frac{\hbar}{j}\frac{\partial}{\partial t}\psi_0(\boldsymbol{r},t) \tag{6}$$

where m_0 is the rest mass of the free electron and is 9.11×10^{-31} kg, and $\tilde{N}$ is equal to $h/2\,\pi$, where Planck's constant h is 6.625×10^{-34} J·s. The wave function $\psi_0(r,t)$ is a complex quantity, and its squared magnitude represents the probability of finding the carrier at a point r and time t. The subscript 0 is used to distinguish ψ_0 from the ψ we will use later to define the effective mass. The sum of probabilities of a large number of electrons at a time t is interpreted as the probability density of the electron.

To solve Eq. (6) one needs to model the potential energy $U(\boldsymbol{r},t)$, which is composed of two parts: the microscopic part due to the periodic lattice of ions and other electrons, and the macroscopic part due to the external field $U_E(\boldsymbol{r},t)$. The microscopic part itself consists of two contributions: one due to the periodic ionic lattice, $U_L(r,t)$, and the scattering potential due to electrons, defects, phonons, and impurities, $U_S(\boldsymbol{r},t)$. Thus, the total potential energy can be written as (5)

$$U(\boldsymbol{r},t) = U_L(\boldsymbol{r},t) + U_S(\boldsymbol{r},t) + U_E(\boldsymbol{r},t) \tag{7}$$

A schematic illustration of the three contributions to the potential energy is shown in Fig. 1.

To simplify the solution of Eq. (6), we consider the simple case of the periodic potential $U_L(\boldsymbol{r},t)$ and neglect $U_S(\boldsymbol{r},t)$ and $U_E(\boldsymbol{r},t)$. The periodicity of the crystal potential results in a periodic eigenfunction solution to the Schrödinger equation, and the wave functions will be Bloch waves. See Pierret (6) for a complete discussion of the Bloch theorem and Bloch waves. The wave function of an electron in a

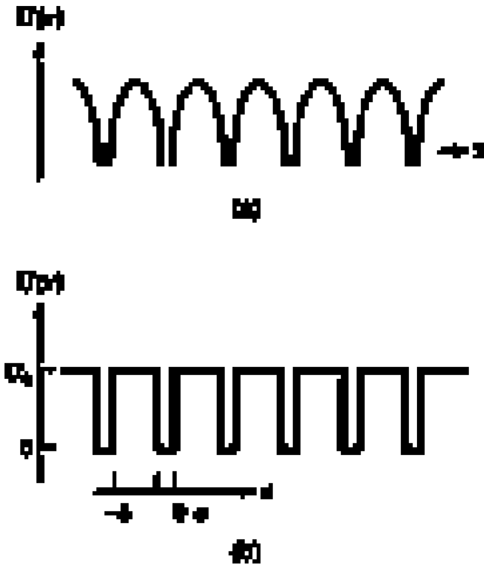

Figure 2. A one-dimensional potential energy of a crystalline lattice: (a) periodic potential, (b) Kronig–Penny model.

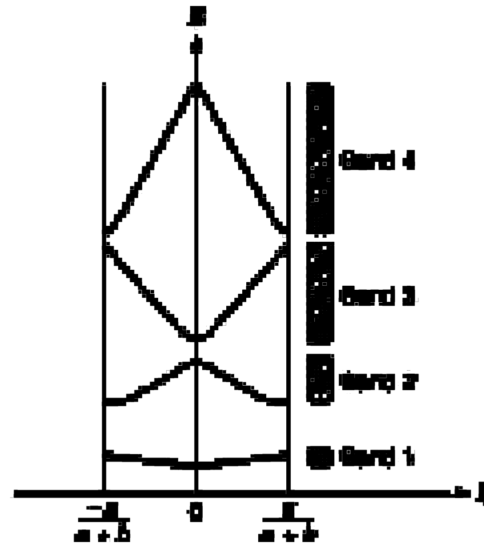

Figure 3. Energy–momentum diagram of allowed $E(k)$ states in the first Brillouin zone of a one-dimensional crystal as determined from the Kronig–Penny model. After Pierret (6); reprinted with permission.

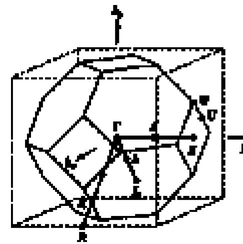

Figure 4. First Brillouin zone for materials crystallizing in the diamond and zinc blende lattices. After Pierret (6); originally after Blakemore (10); reprinted with permission.

band ν with wave vector, $\boldsymbol{k}$ is given by

$$\psi_0(\boldsymbol{r}, t) = u_{\nu,\boldsymbol{k}}(\boldsymbol{r}) \exp(i\boldsymbol{k}\cdot\boldsymbol{r}) \exp\left(-\frac{jE_\nu(\boldsymbol{k})t}{\hbar}\right) \tag{8}$$

where $u_{\nu,k}(\boldsymbol{r})$ are the Bloch functions, which have the same periodicity as the crystal lattice and are different for each ν and each $\boldsymbol{k}$. The plots of $E_\nu(\boldsymbol{k})$ are known as the *energy band diagrams*.

Even with the simplifications described above, the solution of the Schrödinger equation for an electron in a crystal remains formidable. A further simplification, referred to as the Kronig–Penny model, is achieved by approximating the real periodic crystal potential shown in Fig. 2(a) with that in Fig. 2(b). The mathematical details of the Kronig–Penny model are rather straightforward and can be found in many references (see for example, Refs. 6, 7, or 4). The resulting $E(k)$ relationships for the first four bands are depicted in Fig. 3. The range of k from $-\pi/(a + b)$ to $\pi/(a + b)$ forms the first *Brillouin zone*. Note that the group velocity of electrons, defined as $(1/\tilde{N})\ dE/dk$, is zero at the zone boundaries. This implies that electrons with such energy and momentum will simply be standing waves.

The concept of the one-dimensional energy band diagram can be readily extended to three dimensions in which case the Brillouin zone becomes a three-dimensional volume in k-space enclosing the k values associated with a given energy band. The first 3-D Brillouin zone for a diamond cubic (Si, Ge) or zinc blende crystal is an octahedron truncated by [100] planes at a distance of $2\ \pi/a$ from the center of the zone, where a is the cubic lattice constant. This is illustrated in Fig. 4. The zone center, point Γ, corresponds to $\boldsymbol{k} = \mathbf{0}$ and is a point of high symmetry. Other points of high symmetry are the X and the L points, which correspond to ends of the zone along the $\langle 100\rangle$ and $\langle 111\rangle$ directions, respectively. (The notation $\langle\ \rangle$ indicates the equivalent directions of certain planes in the crystal. For example, in the cubic crystal the direction $\langle 100\rangle$ is the direction perpendicular to a plane that intercepts the x axis at the point with x coordinate 1, and parallel to the yz plane.)

The distance from the Γ point to the X point is more than that from the Γ point to the L point. The ratio of these distances is in fact $\sqrt{3}$ Since plotting a complete $E(\boldsymbol{k})$ diagram requires four dimensions (i.e., E, k_x, k_y, k_z), it is customary to depict projected $E(k)$ plots along certain physically important $\boldsymbol{k}$ directions, which are typically the directions of high symmetry. Plots of projected $E(k)$ diagrams are shown in Fig. 5(a) for germanium, 5(b) for silicon, and 5(c) and 5(d) for gallium arsenide in the $\langle 100\rangle$ and $\langle 111\rangle$ directions.

The $E(k)$ curves above the point marked E_c are for electrons (with energy increasing upward) and are called the conduction band. The $E(k)$ curves below the point marked E_v are called valence bands and are for holes (with energy increasing downward). For most semiconductors, the points, Γ, L, and X are of importance, as they exhibit valleys (energy minima) for electrons and peaks (energy maxima) for holes, and most of the electrons populate the states at the bottom of the valleys, whereas most of the holes reside at the top of the peaks.

The energy difference between the maximum of the valence band (the Γ point) and the minimum of the conduction

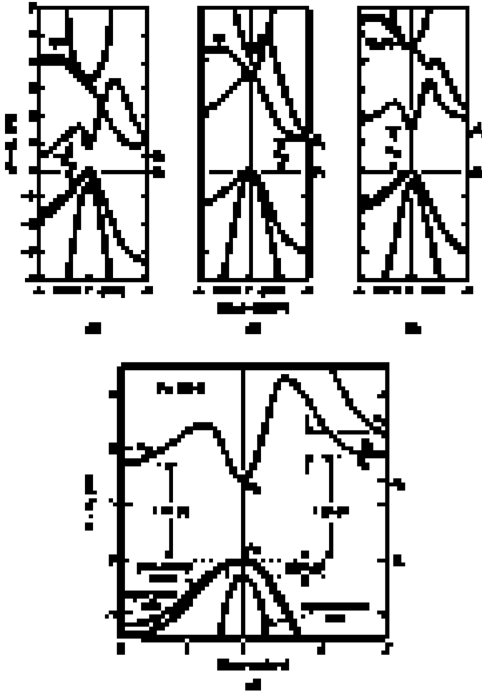

Figure 5. $E(k)$ diagrams characterizing the conduction and valence bands of (a) germanium, (b) silicon, (c) gallium arsenide, and (d) gallium arsenide in more detail. After Pierret (6); originally (a–c) after Sze (11) and (d) after Blakemore (10); reprinted with permission.

band is called the *bandgap* of the semiconductor:

$$E_g = E_c - E_v \tag{9}$$

The parameter E_g is perhaps the single most important parameter of any semiconducting material. Many of the optical and electronic properties of semiconductors are related to the bandgap. The minimum in the conduction band for Ge and Si occurs at the L and X points, respectively. Since the valence band maximum and the conduction band minimum are not at the same k value, these materials are called *indirect bandgap* semiconductors. In such materials, any electronic transition between the top of the valence band the bottom of the conduction band (i.e. generation and recombination) requires the exchange of both energy and momentum. In GaAs, the maximum in the valence band and the minimum in the conduction band occur at the Γ point, and any electronic transitions between the valence band maximum and conduction band minimum do not require exchange of momentum. Thus, GaAs is called a *direct bandgap* material. The L valley of GaAs is situated only 0.3 eV above the Γ valley, and application of high-electric-field results in transfer of carriers from the Γ valley to the L valley. This phenomenon is the basis of many transferred-electron devices, such as the Gunn diode. Finally, the valence band of most semiconductors at the Γ point has two $E(k)$ curves, and the valence electrons are degenerate, which leads to the concept of light and heavy holes, which will be discussed in the next section.

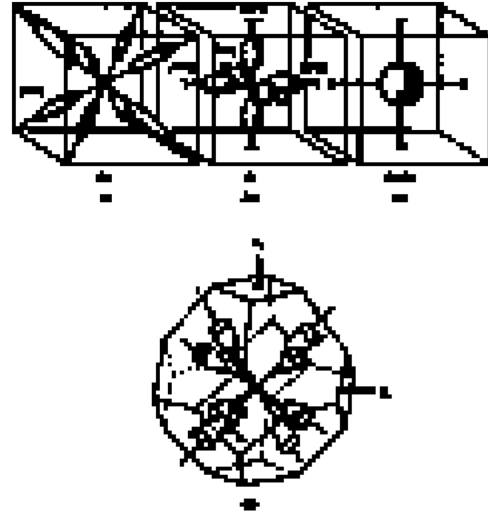

Figure 6. Constant-energy surfaces characterizing the band structure of (a) germanium, (b) silicon, (c) gallium arsenide, and (d) germanium, showing the truncation of the surfaces at the Brillouin zone boundaries. After Pierret (6); originally (a–c) after Sze (11) and Ziman (12), (d) after McKelvey (13); reprinted with permission.

EFFECTIVE MASS OF CARRIERS

The $E(\boldsymbol{k})$ diagrams discussed in the preceding sections are plotted in $\boldsymbol{k}$ space. An alternative approach is to plot all $\boldsymbol{k}$ values that result in the same energy, to form the *constant-energy surface*. Usually, the energy of the surface is chosen to be close the bottom of the conduction band or the top of the valence band, as that corresponds to the carriers that take part in transitions and transport. Figure 6 depicts the constant-energy surfaces for the conduction bands of Ge, Si, and GaAs for energies near E_c. In the $E(\boldsymbol{k})$ diagram of Ge, the conduction band minimum occurs along each of the eight equivalent $\langle 111 \rangle$ directions. This is shown in Fig. 6(a) and 6(d). Thus, the constant-energy surface consists of eight elongated ellipsoids. In Si, there are six ellipsoids because of the six equivalent $\langle 100 \rangle$ directions in the $E(\boldsymbol{k})$ diagram along which the conduction band minimum occurs. Since the conduction band minimum occurs in GaAs at the Γ point, the constant-energy surface is a sphere centered at $\boldsymbol{k} = \boldsymbol{0}$. Upon the development of the effective-mass concept, one will have a better appreciation of the usefulness of the constant-energy surfaces.

In one dimension let us consider the classical electron with a velocity v as a wave packet with a group velocity v_g as given by

$$v_g = \frac{1}{\hbar}\frac{dE}{dk} \tag{10}$$

When an external force acts on the wave packet for a short time dt, the energy of the packet increases by an amount dE given by

$$dE = F\,dx = Fv_g\,dt \tag{11}$$

from classical Newtonian mechanics. Equivalently, we can write Eq. (11) as

$$\begin{aligned} F &= \frac{1}{v_g}\frac{dE}{dt} \\ &= \frac{1}{v_g}\frac{dE}{dk}\frac{dk}{dt} \end{aligned} \tag{12}$$

Differentiating Eq. (10) with respect to time yields

$$\begin{aligned} \frac{dv_g}{dt} &= \frac{1}{\hbar}\frac{d}{dt}\frac{dE}{dk} \\ &= \frac{1}{\hbar^2}\frac{d^2E}{dk^2}\frac{d(\hbar k)}{dt} \end{aligned} \tag{13}$$

Solving for $d(\tilde{N}k)/dt$ results in

$$\begin{aligned} \frac{d(\hbar k)}{dt} &= \frac{dv_g}{dt}\frac{1}{\dfrac{1}{\hbar^2}\dfrac{d^2E}{dk^2}} \\ &= F \\ &= m^*\frac{dv_g}{dt} \end{aligned} \tag{14}$$

Thus, we have

$$m^* = \frac{1}{\dfrac{1}{\hbar^2}\dfrac{d^2E}{dk^2}} \tag{15}$$

The above equation defines the *effective mass* of carriers, m^*, as a parameter obtained from the inverse curvature of the $E(k)$ relationship. Use of the effective mass allows for lumping together all the quantum mechanical effects due to the crystal potential into the carrier's mass, so that in transport calculations there is no need to consider the quantum effects of the crystal potential.

Extending the effective mass concept to 3-D crystal results in an effective-mass tensor given by (6)

$$\frac{1}{m^*} = \begin{pmatrix} m_{xx}^{-1} & m_{xy}^{-1} & m_{xz}^{-1} \\ m_{yx}^{-1} & m_{yy}^{-1} & m_{yz}^{-1} \\ m_{zx}^{-1} & m_{zy}^{-1} & m_{zz}^{-1} \end{pmatrix} \tag{16}$$

where

$$\frac{1}{m_{ij}} = \frac{1}{\hbar^2}\frac{\partial^2 E}{\partial k_i \partial k_j} \quad i, j = x, y, z \tag{17}$$

with $i, j = x,y,z$. Since the $E(\boldsymbol{k})$ relationships for all semiconductors are parabolic about the band extrema, all off-diagonal components are zero.

Let us relate the effective mass to the constant-energy surfaces discussed above. For GaAs, with spherical constant-energy surface for energies near the conduction band minimum (Γ point), the $E(\boldsymbol{k})$ relationship can be written as

$$E - E_C = A(k_x^2 + k_y^2 + k_z^2) \tag{18}$$

The diagonal components of the effective-mass tensor will be given by

$$m_{xx}^{-1} = m_{yy}^{-1} = m_{zz}^{-1} = \frac{2A}{\hbar^2} = \frac{1}{m_e^*} \tag{19}$$

Also, Eq. (18) can be written as

$$E - E_C = \frac{\hbar^2}{2m_e^*}(k_x^2 + k_y^2 + k_z^2) \tag{20}$$

where m_e^* is the common value of the three diagonal components, and the effective-mass tensor reduces to a simple scalar. Thus, in GaAs, the transport is characterized by an orientation-independent effective mass. The importance of the shape of the constant-energy surface (spherical versus ellipsoidal) will become apparent when we developed the concept of mobility later on in this article.

The constant-energy surfaces of Si and Ge are elongated ellipsoids:

$$E - E_C = Ak_1^2 + B(k_2^2 + k_3^2) \tag{21}$$

where k_1, k_2, and k_3 are the principal axes, with k_1 along the axis of rotation connecting the two extrema of the elongated ellipsoid together. [See Fig. 6(a) and 6(b).] The off-diagonal components of the mass tensor are again zero. The three nonzero diagonal components are

$$m_{11}^{-1} = \frac{2A}{\hbar^2} \tag{22}$$

$$\begin{aligned} m_{22}^{-1} &= m_{33}^{-1} \\ &= \frac{2B}{\hbar^2} \end{aligned} \tag{23}$$

The component m_{11}, associated with the axis of rotation, is called the *longitudinal effective mass* and is denoted as m_l^*. The components m_{22} and m_{33}, which are the effective masses in the two perpendicular directions to the axis of rotation, are equal and are called the *transverse effective mass* and are denoted as m_t^*. Equation (21) can then be written in terms of m_l^* and m_t^* as

$$E - E_C = \frac{\hbar^2}{2m_l^*}k_1^2 + \frac{\hbar^2}{2m_t^*}(k_2^2 + k_3^2) \tag{24}$$

Thus, for Si and Ge, the two effective masses m_l^* and m_t^* characterize the transport of electrons in the conduction band. The ratio m_l^*/m_t^* is given by (6)

$$\frac{m_l^*}{m_t^*} = \frac{L_r}{W_m} \tag{25}$$

where L_r is the length of the ellipsoid along the axis of rotation and W_m is the maximum width of the ellipsoid perpendicular to the axis of rotation. It is obvious that for both Si and Ge, m_l^* is always greater than m_t^*.

Using the $E(k)$ curves for electrons in the valence band, one can define two effective masses for holes in Ge, Si, and GaAs. (Actually, the third band, called the split-off band, is seldom populated and therefore is not usually considered.) These two effective masses are the light-hole effective mass m_{lh}^* and the heavy-hole effective mass m_{hh}^*, which correspond to the two $E(k)$ curves in the valence bands of the three semiconductors shown in Fig. 5.

Figure 7. A linear monoatomic chain where the sth atom is displaced by an amount u_s. The interatomic forces are represented by springs. The interatomic spacing is a.

PHONONS AND LATTICE DYNAMICS

At any temperature above 0 K, the atoms forming the crystal are subject to a random thermal motion that affects the movement of carriers within the crystal. One might consider the crystal as a chain of solid balls attached together with deformable springs upon which an oscillatory wave of thermal motion is imposed. This constant random thermal motion is the main scattering mechanism that impedes the movement of carriers in many semiconductor materials. The energy and frequency of this thermal vibration can be characterize by the concept of *phonons* in much the same way the *photons* characterize the electromagnetic radiation. Just as photons are quanta of radiation energy, phonons are quanta of thermal vibration energy.

It is through the interaction of phonons with electrons that the mobility of carriers in a semiconductor is limited. The exchange of energy between the carriers and the lattice can take place through the either the emission or absorption of a phonon. Many factors influence the frequency and momentum of the phonons in a crystal, including the deformability of the crystal, the number of atoms in the primitive cell of the crystal, the atomic mass of the constituent atoms, and other factors. Depending upon the frequency of the phonons, they are grouped into *acoustic* (low frequency) and *optical* (high frequency). The optical phonons are either *polar* or *nonpolar*, according as the bonds in the crystal are purely covalent or slightly ionic. Both acoustic and optical phonons can be *longitudinal* or *transverse*, according as the vibration of the atoms is perpendicular or parallel to the direction of propagation of the wave.

It should be pointed out that this random thermal motion of atoms, no matter how intense it may become, does not result in a net movement of the crystal atoms, as they only vibrate around a stationary equilibrium point.

A simple one-dimensional monatomic model for phonons in Ge and Si can be developed if we make the following simplifying assumptions: (1) only the motion of nearest neighbors (in a linear chain of atoms) is significant, and (2) the covalent bonds are considered as linear springs in which the displacement is linearly proportional to the force. Referring to Fig. 7, and denoting the displacement of the sth atom as u_s, one can easily write the following differential equation for the motion of the sth atom:

$$M\frac{d^2u_s}{dt^2} = F_s = C(u_{s+1} - u_s) - C(u_{s-1} - u_s) \tag{26}$$

A steady-state solution to Eq. (26) can be tried as

$$u_{s\pm1} = e^{\pm iqa}u_s \tag{27}$$

where a is the lattice constant and q is the momentum wave vector of the lattice (to be distinguished from k, which is the momentum wave vector of the electrons).

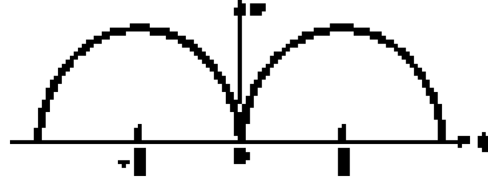

Figure 8. Dispersion relationship for phonons in a monatomic one-dimensional lattice.

Using Eq. (27) in Eq. (26) yields

$$-M^2\omega^2u_s = Cu_s(e^{+iqa} + e^{-iqa} - 2) \tag{28}$$

where

$$\omega^2 = \frac{2C}{M}(1 - \cos\ qa) \tag{29}$$

where q, the lattice (or phonon) wave vector, is limited to $-\pi/a \le q \le \pi/a$. Equation (29) can be written as

$$\omega = 2\sqrt{\frac{C}{M}}\sin\frac{qa}{2} \tag{30}$$

which relates the frequency of phonons to their momenta, is called the *dispersion curve of phonons*, and is plotted in Fig. 8. For small wave vectors q, the sinusoid in Eq. (30) can be expanded so that

$$\omega = a\left(\frac{C}{M}\right)^{1/2}q \tag{31}$$

which is similar to the frequency of a sound wave moving through the lattice. In fact the velocity of the sound waves through the lattice can be written as

$$v_s = a\left(\frac{C}{M}\right)^{1/2} \tag{32}$$

By measuring the sound velocity of an acoustic wave through the lattice, one may determine the "spring" constant C.

The mathematics of extending this concept to a diatomic chain (such as GaAs) is only slightly more elaborate. The resulting phonon dispersion relationship is, however, significantly more involved (4):

$$\omega^4 - 2C\left(\frac{M_1+M_2}{M_1M_2}\right)\omega^2 + 2\frac{C^2}{M_1M_2}(1 - \cos\ qa) = 0 \tag{33}$$

where M_1 and M_2 are the masses of the two atoms, and a is the lattice constant. Now there are two values of ω for each value of q. One is a low-frequency branch, which is called the *acoustic branch*, and the other is high-frequency branch (in the infrared part of the optical frequency spectrum), which is called the *optical branch*. The dispersion relation for the diatomic lattice is shown in Fig. 9. For the case of wave vector $q = 0$, the phonon waves become static standing waves with frequencies

$$\omega = 0 \tag{34}$$

and

$$\omega = \left(2C\frac{M_1+M_2}{M_1M_2}\right)^{1/2} \tag{35}$$

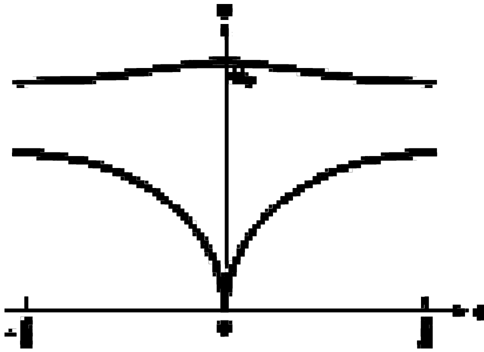

Figure 9. Dispersion relation for phonons in a diatomic one-dimensional lattice. The low-frequency phonons are the accoustic branch, and the high-frequency phonons are the optical branch.

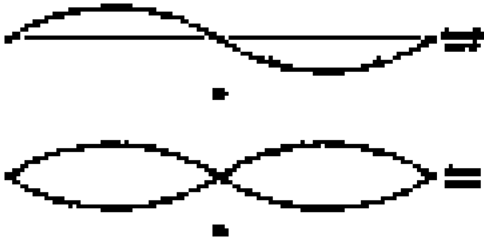

Figure 10. Vibrations of a diatomic chain. (a) In the acoustic mode the two atoms M_1 and M_2 are vibrating together, whereas (b) in the optical mode they are vibrating against each other.

for the acoustic mode and the optical mode, respectively. This mode of vibration corresponds to the static displacement of the atoms of mass M_2 relative to the atoms of mass M_1. In this mode of vibration, the two types of atoms are rigidly shifted with respect to each other. For nonzero small values of q, the two chains of atoms, while rigidly vibrating against each other, both remain in motion. (See Fig. 10).

For higher values of q (corresponding to shorter wavelengths) and in the limiting case of $q = \pi/a$, the dispersion relation becomes

$$\omega^4 - 2C\left(\frac{M_1+M_2}{M_1M_2}\right)\omega^2 + \frac{4C^2}{M_1M_2} = 0 \tag{36}$$

which has two solutions:

$$\omega_1 = \left(\frac{2C}{M_1}\right)^{1/2} \tag{37}$$

and

$$\omega_2 = \left(\frac{2C}{M_2}\right)^{1/2} \tag{38}$$

The two frequencies each involve only a single mass. The first frequency, ω_1, corresponds to the vibration of atoms of type M_1 while the M_2 chain is at rest, and the second frequency, ω_2, to the M_2 chain vibrating while the M_1 chain is at rest. The larger the mass, the lower is the frequency of vibration.

Figure 10 depicts the acoustic and optical modes of vibration of a diatomic chain. In acoustic mode, the entire collective chain of the two atoms M_1 and M_2 is vibrating,

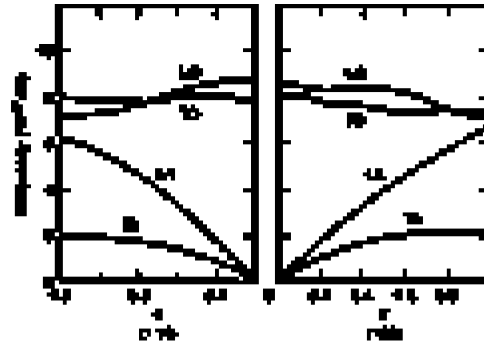

Figure 11. Dispersion curves for GaAs in ⟨111⟩ and ⟨100⟩ directions. Various branches are depicted: transverse accoustic (TA), longitudinal accoustic (LA), transverse optical (TO), and longitudinal optical (LO). After Ferry (4); originally after Waugh and Dolling (14); reprinted with permission.

but in the optical mode, the atoms M_1 and M_2 are vibrating against each other. The dispersion relations [$f(q)$ plots] can also be plotted for different directions in the crystals, usually for points of principal symmetry. Figure 11 shows the phonon $f(q)$ plots for GaAs in the Γ direction. Each of the two acoustic and optical modes is split into longitudinal and transverse branches, which are marked LA, TA, LO, and TO. The range of vibration frequencies of all phonons in many semiconductors is between 10^{12} Hz and about 5×10^{13} Hz.

SCATTERING PHENOMENON AND FERMI "GOLDEN RULE"

The transport of electrons (and holes) in a crystal is impeded (and also, remarkably, assisted) by scattering forces. The scattering processes, on one hand, limit the velocity of the carriers and give rise to the so-called *saturation velocity*. On the other hand, without scattering processes, the applied external force causes the momentum of electrons to increase uniformly, causing the electrons to cycle through the Brillouin zone without a net average velocity. The resulting phenomenon is called *Bloch Oscillations*. Indeed, transport is a balance between the accelerative forces (the external applied field, for example) and the dissipative forces, which are the scattering forces.

The adiabatic approximation discussed above in the section "Approximating the Dynamics of Real Electrons in Real Crystals" allows separation of ion core electrons and valence electrons. The thermal motion of ion core electrons constitutes the lattice vibrations (formation of phonons). It is the interaction of the electrons with these phonons that makes the greatest contribution to the scattering (and consequently to the mobility) of carriers in semiconductors. This interaction can be between electrons and different branches of phonons, including acoustic phonons and polar and nonpolar optical phonons. There are also nonphonon scattering processes, such as ionized impurity scattering, alloy scattering, surface roughness scattering, piezoelectric scattering, neutral impurity scattering, and intervalley scattering.

Lundstrom (8) classifies the carrier scattering mechanisms as:

Scattering by defects:
- Neutral impurities
- Dislocations
- Alloy scattering
- Ionized impurities

Scattering by carriers:
- Binary electron–electron
- Binary electron-hole
- Collective plasmons

Scattering by phonons:
- Acoustic deformation potential
- Optical deformation potential
- Acoustic polar
- Optical polar

Which scattering mechanism dominates the transport of carriers in a semiconductor depends on a number of factors, including (1) the crystal lattice temperature, (2) the intensity of the applied external field, (3) the impurity doping level within the crystal, (4) the amount of injection of external carriers (excess carriers), (5) the orientation of the crystal, (6) the shape of the constant-energy surfaces in the band structure of the crystal (spherical or ellipsoidal), (7) the type of junction (homojunction or heterojunction) the crystal is used for, and other factors.

The scattering mechanisms influence the transport of a charged particle through a *scattering potential*, which can exhibit spatial (and temporal) dependence. For example, the scattering potential U_S for ionized impurity scattering is given by (8)

$$U_S = \frac{q^2}{4\pi\kappa_s\epsilon_0 r} e^{-r/L_D} \tag{39}$$

where $\kappa_s\ \varepsilon_0$ is the dielectric constant of the semiconductor and L_D is the Debye length given by

$$L_D = \sqrt{\frac{\kappa_s\epsilon_0 k_B T_L}{q^2 n_0}} \tag{40}$$

where k_B is the Boltzmann constant, T_L is the lattice temperature in kelvin, and n_0 is the electron concentration. Scattering potentials for other scattering mechanisms are given in the section after next.

The scattering rate $S(\boldsymbol{p}, \boldsymbol{p}')$, can be completely described using the initial and final momentum vector states, $\boldsymbol{p}$ and $\boldsymbol{p}'$. It should be noted that we make the distinction between $\boldsymbol{p}$, which is the *crystal* momentum state, and $\boldsymbol{k}$, which is *electron* momentum state. Fermi's "golden rule," which is based on a first-order perturbation of Schrödinger's equation, provides the relationship between scattering rate and scattering potential. Given the scattering potential of a scattering source, the scattering rate $S(\boldsymbol{p}, \boldsymbol{p}')$ is given by

$$S(\boldsymbol{p}, \boldsymbol{p}') = \frac{2\pi}{\hbar} |H_{\boldsymbol{p},\boldsymbol{p}'}|^2 \delta(E(\boldsymbol{p}') - E(\boldsymbol{p}) - \hbar\omega) \tag{41}$$

The matrix element, $|H_{p,p'}|^2$, is a volume integral involving the scattering potential U_s and the wave functions describing the initial and final states of the carrier, $\psi(\boldsymbol{p})$ and $\psi(\boldsymbol{p}')$, respectively:

$$H_{\boldsymbol{p},\boldsymbol{p}'} = \int_{-\infty}^{\infty} \psi^*(\boldsymbol{p}') U_s \psi(\boldsymbol{p})\, dV \tag{42}$$

The δ function in Eq. (41) ensures that the energy is conserved during the scattering process and thus involves the initial and final energies of the carrier, $E(\boldsymbol{p})$ and $E(\boldsymbol{p}')$, respectively. The energy of the scatterer is $\tilde{N}\ \omega$, with ω as the angular frequency of the scatterer. Once the scattering potential is identified, Fermi's "golden rule" provides the scattering rate. The scattering rates due to ionized impurities and several branches of phonons are described in the section after next.

Even though Fermi's "golden rule" is widely used in device modeling, it has several limitations (4,5,8). Firstly, it assumes that the scattering is instantaneous and spatially localized. Secondly, it is assumed that the scattering from the initial momentum state is weak and hence the occupation probability of that state is approximately unity throughout the scattering process, which is the Born approximation discussed earlier. Additionally, it assumes that the scattering event is infrequent, which may not be true, especially at high temperatures and high doping. In the next sections we illustrate the use of Fermi's "golden rule" in the calculation of scattering rates of several scattering sources.

SCATTERING RELAXATION TIMES

The scattering rates described by Fermi's "golden rule" can be used to define some characteristic terms (referred to as relaxation times) that are related to the transition rate of carriers due to scattering. These relaxation times are time intervals within which the scattering sources completely randomize the momentum or energy of the ensemble of carriers. To arrive at these relaxation times, we consider a small ensemble of electrons (being externally injected into the semiconductor) each with initial momentum $\boldsymbol{p}_0$, as shown in Fig. 12(a). The notion of relaxation is used in the sense of the initial momentum (or energy) being relaxed (or dissipated) by scattering agents within the crystal. Let us assume that the electrons undergo collisions with any one of the scattering sources such that they are scattered to the final state $\boldsymbol{p}'$. We define the scattering rate as (8)

$$\frac{1}{\tau(\boldsymbol{p}_0)} = \sum_{\boldsymbol{p}'\|} S(\boldsymbol{p}_0, \boldsymbol{p}') \tag{43}$$

where $\boldsymbol{p}'\|$ denotes summation over all final states $\boldsymbol{p}'$. Note that only the states whose spins are parallel to that of the incident carriers are considered. At time $t = \tau(\boldsymbol{p}_0)$, for nonisotropic scattering mechanisms, the carriers retain a memory of their incident momentum, as shown in Fig. 12(b). If we weight each collision by the fraction of change in momentum (in the direction of the incident initial mo-

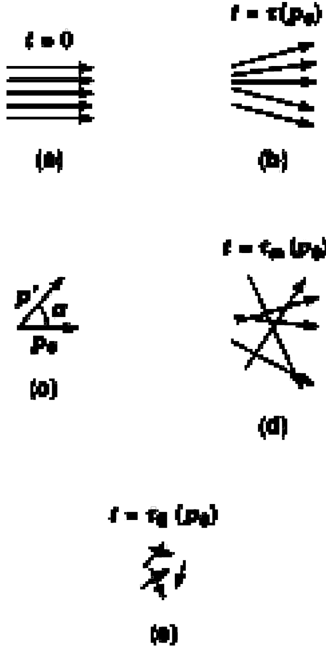

Figure 12. Illustration of the process of relaxation of the momentum and energy of an ensemble of electrons injected into a crystal. (a) An initial group of electrons with momentum $\boldsymbol{p}_0$ are injected at time $t = t_0$. (b) At time $t = \tau(\boldsymbol{p}_0)$ the carriers are scattered, but they retain a memory of their incident momenta. (c) The polar angle a between the incident ($\boldsymbol{p}_0$) and scattered ($\boldsymbol{p}'$) momenta. (d) At time $t = \tau_{\mathrm{m}}(p_0)$ the momentum of the carriers has been completely randomized by the scatterers. (e) At time $t = \tau_{\mathrm{E}}(p_0)$ the initial energy of the ensemble has been dissipated by the scattering sources, as indicated by the reduced momentum vectors. After Lundstrom (8); reprinted with permission.

mentum which is along the z axis) as

$$\frac{1}{\tau_{\mathrm{m}}(\boldsymbol{p}_0)} = \sum_{\boldsymbol{p}'\|} S(\boldsymbol{p}_0, \boldsymbol{p}') \left(1 - \frac{p'_z}{p_{z0}}\right) \tag{44}$$

then $\tau_{\mathrm{m}}(p)$ will be the *momentum relaxation time* and will be given by

$$\frac{1}{\tau_{\mathrm{m}}(\boldsymbol{p}_0)} = \sum_{\boldsymbol{p}'\|} S(\boldsymbol{p}_0, \boldsymbol{p}') \left(1 - \frac{p'}{p_0}\cos\alpha\right) \tag{45}$$

where α is the polar angle between the incident and scattered momenta, as shown in Fig. 12(c). At time $t = \tau_{\mathrm{m}}(\boldsymbol{p}_0)$, the scattering source has completely randomized the electrons' momenta. The quantity $1/\tau_{\mathrm{m}}(\boldsymbol{p}_0)$ is the momentum relaxation rate. Its reciprocal, $\tau_{\mathrm{m}}(\boldsymbol{p}_0)$, is the characteristic time for relaxation (randomization) of injected initial momentum, as depicted in Fig. 12(d).

It is possible to relax the injected momentum without affecting the energy of the carriers. However, some scattering mechanisms relax (dissipate) the energy of the injected carriers within a time interval, $\tau_{\mathrm{E}}(\boldsymbol{p}_0)$, referred to as *energy relaxation time*. This is shown in Fig. 12(e), where the lengths of the momentum vectors have been reduced to indicate the dissipation of the carriers' energy to the crystal by the action of scatterers. The energy relaxation time is defined (much like the momentum relaxation time) by weighting each collision by the fraction of change in energy. This will result in (8)

$$\frac{1}{\tau_{\mathrm{E}}(\boldsymbol{p}_0)} = \sum_{\boldsymbol{p}'\|} S(\boldsymbol{p}_0, \boldsymbol{p}') \left(1 - \frac{E(\boldsymbol{p}')}{E(\boldsymbol{p}_0)}\right) \tag{46}$$

where $\tau_{\mathrm{E}}(\boldsymbol{p}_0)$ is the energy relaxation time, and $1/\tau_{\mathrm{E}}(\boldsymbol{p}_0)$ is the energy relaxation rate of carriers.

The three relaxation times τ, τ_{m}, and τ_{E} provide a foundation for solution of Boltzmann transport equation, which is described in. The relaxation times are also used to define one of the most widely used parameters for transport in semiconductors, referred to as *mobility*, which is discussed in the section after next.

SCATTERING RATES FROM FERMI'S GOLDEN RULE

In this section, we will discuss ionized impurity scattering and phonon scattering. The reader is referred to Refs. 4, 8, and 9 for comprehensive advanced treatment of these and other scattering mechanisms in Si and GaAs semiconductors.

Ionized Impurity Scattering Rates

Fermi's golden rule relates the scattering rate $S(\boldsymbol{p}, \boldsymbol{p}')$ to the scattering potential U_s as

$$S(\boldsymbol{p}, \boldsymbol{p}') = \frac{2\pi}{\hbar} |H_{\boldsymbol{p}'\boldsymbol{p}}|^2 \delta(E(\boldsymbol{p}') - E(\boldsymbol{p}) \pm \hbar\omega) \tag{47}$$

with the matrix element $H_{p'p}$ given by

$$H_{\boldsymbol{p}'\boldsymbol{p}} = \int_{-\infty}^{+\infty} \psi^*_{\boldsymbol{p}'}(z) U_{\mathrm{S}}(z,t) \psi_{\boldsymbol{p}}(z)\, dz \tag{48}$$

The scattering potential U_{S} for an ionized impurity is assumed to be a screened Coulombic potential given by (8)

$$U_{\mathrm{S}}(r) = \frac{q^2}{4\pi\kappa_{\mathrm{s}}\epsilon_0 r} e^{-r/L_{\mathrm{D}}} \tag{49}$$

where the screening length L_{D} is the Debye length. In regions such as the depletion region of a *pn* junction where the carrier density is low, the screening is minimal and the Coulombic potential is unscreened:

$$U_{\mathrm{S}}(r) = \frac{q^2}{4\pi\kappa_{\mathrm{s}}\epsilon_0 r} \tag{50}$$

Using Eq. (49) in Eq. (47), and working out the integration in spherical coordinates, we find the scattering rate to be (8)

$$S(\boldsymbol{p}, \boldsymbol{p}') = \frac{2\pi N_{\mathrm{I}} q^4}{\hbar\kappa_{\mathrm{s}}^2\epsilon_0^2\Omega} \frac{\delta(E(\boldsymbol{p}') - E(\boldsymbol{p}))}{[4(p/\hbar)^2\sin^2(\alpha/2) + (1/L_{\mathrm{D}}^2)]^2} \tag{51}$$

where Ω is the volume of the crystal and α is the angle between $\boldsymbol{p}$ and $\boldsymbol{p}'$. N_T is the concentration of ionized impurities. Typically the scattering decreases with increasing energy, which can be associated with less interaction time between the scatterer and carrier.

For weakly screened scattering potentials (such as the ones encountered in regions of very low doping, or in the

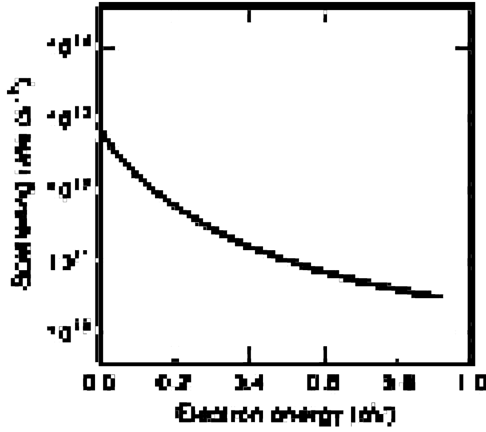

Figure 13. A schematic plot of ionized impurity scattering rate versus electron energy.

space charge regions of *pn* junctions) the screened Debye length L_D tends to infinity and the scattering rate will be

$$S(\boldsymbol{p},\boldsymbol{p}') = \frac{2\pi N_I q^4}{\hbar\kappa_s^2\epsilon_0^2\Omega[2p/\hbar)^4\sin^4(\alpha/2)]^2}\,\delta(E'-E) \tag{52}$$

The difference between screened and unscreened ionized impurity scattering rates becomes apparent only when the polar angle between $\boldsymbol{p}$ and $\boldsymbol{p}'$ is extremely small. But for both cases, the scattering rate decreases with increasing carrier energy, implying that ionized impurities tend to scatter the carriers with lower kinetic energies. This is simply because the rapidly moving carriers are deflected less by ionized impurities. The momentum relaxation time for screened ionized impurity scattering can be worked out to be (8)

$$\tau_m(p) = \frac{16\sqrt{2m^*}\pi\kappa_s^2\epsilon_0^2}{N_I q^4}\left[\ln(1+\gamma^2) - \frac{\gamma^2}{1+\gamma^2}\right]^{-1} E^{3/2}(p) \tag{53}$$

where $\gamma = 8m^*E(p)L^2{}_D/\tilde{N}^2$.

A plot of $1/t_m(p)$ versus energy is shown in Fig. 13. As can be seen, the carriers with higher kinetic energy have longer momentum relaxation time, implying that the ionized impurities have less scattering effect on high-energy carriers. Therefore, under high-electric-field or high-temperature operation, the ionized impurity scattering is expected to be less influential on the transport of carriers.

Similar expressions for momentum relaxation time are obtained for unscreened ionized impurity scattering potentials (8).

The above expression for the momentum relaxation time has constant terms as well as slowly varying terms. A convenient way of expressing the energy and temperature dependence of the relaxation time is of the form

$$\tau_m(p) = \tau_0\left(\frac{E}{kT}\right)^s \tag{54}$$

where τ_0 is approximately constant. Here s is a characteristic exponent that is $s = \sqrt{3}$ for weak to moderate screening, and $s = -½$ for very strong screening.

Phonon Scattering Rates

When a carrier encounters a phonon, the energy and momentum before and after the collision must be conserved:

$$E(\boldsymbol{p}') = E(\boldsymbol{p}) \pm \hbar\omega(\boldsymbol{\beta}) \tag{55}$$

and

$$\boldsymbol{p}' = \boldsymbol{p} \pm \hbar\boldsymbol{\beta} \tag{56}$$

where $\tilde{N}\beta$ is the momentum of the phonon, and the sign is + for the absorption and − for the emission of a phonon. The $\omega(\beta)$ term indicates the momentum dependence of the phonon frequency. For acoustic phonons (AP),

$$\frac{\omega}{\beta} = v_s \tag{57}$$

is the propagation velocity of sound in the crystal. Since $v_s \approx 10^5$ cm/s and the thermal average carrier velocity $v(p) \approx 10^7$ cm/s, then

$$\hbar\beta_{max}(\mathrm{AP}) \approx 2p \tag{58}$$

which indicates that the maximum phonon momentum for elastic acoustic phonon scattering is approximately twice the carrier momentum. The maximum exchange of energy resulting from acoustic phonon scattering is

$$\begin{aligned}\Delta E_{max} &= \hbar\omega_{max}\\ &= \hbar\beta_{max}v_s\\ &\approx 1\,\mathrm{meV}\end{aligned} \tag{59}$$

which is significantly less than the k_BT_L except at very low temperatures (k_BT_L is about 25 meV at room temperature). Therefore, at room temperature, acoustic phonons are treated as being elastic. For optical phonons (OP) the phonon frequency ω is almost momentum-independent, $\omega(\beta) \approx \omega_o$, and the optical phonon energy $\tilde{N}\ \omega_o$ is of the order of tens of meV, which, unlike the acoustic phonon, is comparable to k_BT_L at room temperature. The optical phonons, therefore, unlike the acoustic branch, are inelastic (except for extremely energetic carriers). The maximum optical phonon momentum is (8)

$$\hbar\beta_{max}(\mathrm{OP}) = p\left(1+\sqrt{1\pm\frac{\hbar\omega_o}{E(p)}}\right) \tag{60}$$

Having established the elasticity versus inelasticity of phonon scattering, before we discuss the scattering rates for phonons we need to make a distinction between deformation and polar scattering by phonons. In the section "Phonons and Lattice Dynamics" we illustrated the propagation of lattice vibration throughout the crystal by considering the crystal atoms as attached to their neighbors by deformable springs. It turns out that the crystals of semiconductors, as solid as they appear to be, are indeed deformable structures. When under pressure, the lattice constant a (the dimension of the unit cell) of the crystal changes by a small amount, δa. This small change in turns alters the band structure of the crystal, as depicted in Fig. 14(a). The change in the conduction band and valence band

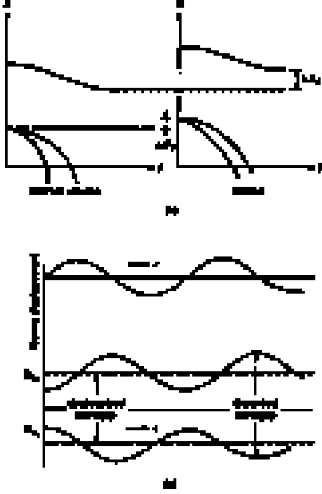

Figure 14. (a) The effect of change in lattice spacing on the band structure of a semiconductor. (b) The effects of lattice deformation, due to a lattice vibration, on the band structure of a semiconductor. After Lundstrom (8); originally (a) after Harrison (15), and (b) after Nag (16); reprinted with permission.

are (8)

$$\delta E_C = D_C \frac{\delta a}{a}$$
$$\delta E_V = D_V \frac{\delta a}{a} \quad (61)$$

where D_C and D_V are the electron and hole acoustic deformation energies and are 9.5 eV and 5 eV in Si, respectively, and 7 eV and 3.5 eV in GaAs, respectively. For these and other scattering parameters (and other transport parameters) of Si and GaAs, see Refs. 8, 9, and 4.

The passage of phonon waves through the crystals deforms the lattice (periodically), causing an alteration in band edges, as shown in Fig. 14(b). This deformation results in interaction of phonons and carrier waves. When an elastic wave $u(x, t)$ is propagating in the crystal, the resulting deformation (scattering of carriers) takes place for both acoustic and optical branches. But, because in the acoustic branch the neighboring atoms are vibrating in the same direction, the change in lattice spacing is produced by the strain $\partial u/\partial x$ and not by the displacement $u(x, t)$. Therefore the scattering potential for acoustic phonon is

$$U_{AP}(x, t) = D_A \frac{\partial u}{\partial x} \quad (62)$$

In the optical branch, in contrast, the neighboring atoms are vibrating in the opposite direction, and the change in lattice spacing is directly related to the propagating displacement as

$$U_{OP}(x, t) = D_O u(x, t) \quad (63)$$

In the above equations D_A and D_0 are acoustic and optical deformation potentials, respectively. The acoustic and optical deformation potentials are the dominant scattering sources in single crystals such as Si. In compound semiconductors, however (such as GaAs, where the bonds between Ga and As atoms are slightly ionic), there is a certain degree of polarity in the atoms of the lattice. This polar nature of the otherwise tetrahedral bonds in the compound semiconductors gives rise to a strong (and dominating) interaction between the carriers and phonons (polar phonons) because of the electric field that is developed in the dipole between two atoms (in GaAs, gallium atoms are slightly negative and arsenic atoms are slightly positive). Polar scattering may be due either to polar acoustic phonons (also referred to as piezoelectric scattering), or to polar optical phonons (*POP*), which is the dominant scattering mechanism in GaAs and other polar semiconductors.

By using the acoustic deformation potential (*ADP*)

$$U_{AP}(x, t) = D_A \frac{\partial u}{\partial x} = \pm i\beta D_A u \quad (64)$$

and the optical deformation potential (*ODP*)

$$U_{OP}(x, t) = D_O u(x, t) = \frac{q q^* u}{i\beta\Omega\epsilon_0} \quad (65)$$

where g^* is the effective change of the dipole and Ω is the volume of the unit cell. Working out the integration prescribed by Fermi's golden rule (8) and incorporating certain quantum mechanical requirements (5), the scattering rates are found to be

$$S(p, p') = \frac{\pi D_A^2 \beta^2}{\rho\omega_s\Omega}(N_{\omega_s} + \tfrac{1}{2} \pm \tfrac{1}{2})\delta(p' - p \mp \hbar\beta)\delta(E' - E \mp \hbar\omega_s) \quad (66)$$

for ADP, and

$$S(p, p') = \frac{\pi D_O^2}{\rho\omega_o\Omega}(N_{\omega_o} + \tfrac{1}{2} \pm \tfrac{1}{2}\delta(p' - p \mp \hbar\beta)\delta(E' - E \mp \hbar\omega_o) \quad (67)$$

for ODP, where D_A carriers acoustic deformation potential
D_O carriers optical deformation potential
$\tilde{N}\ \omega_s$ acoustic phonon energy
$\tilde{N}\ \omega_o$ longitudinal optical phonons energy
$\rho\ \Omega$ mass of the normalization volume
ρ mass density
Ω volume of unit cell
N_{Ω_s} number of acoustic phonons as given by Bose-Einstein distribution
N_{Ω_o} number of optical phonons
½ ± ½ 0 (for phonon absorbed) 1 (for phonon emitted)
$\tilde{N}\beta$ phonon momentum
$\boldsymbol{p}, \boldsymbol{p}'$ carrier momenta before and after collision, respectively

Note that the two scattering rates given by Eq. (66) and Eq. (67) have the dimensions of s^{-1}. This is because the dimension of $D_A^2\,\beta^2$ is the same as that of D_O^2, where D_O and D_A are defined in Eq. (62) and Eq. (63).

Also noteworthy is the lack of any apparent temperature dependence in the above two equations for ADP and ODP. In light of the fact that phonons are heat-generated quanta, one may question this result. The answer lies in the *Bose–Einstein distribution* that relates the number of

phonons to their energy:

$$N_{\boldsymbol{\beta}} = \frac{1}{[e^{\hbar\omega(\boldsymbol{\beta})/k_B T_L} - 1]} \tag{68}$$

which makes both N_{Ω_o} and N_{Ω_s} in Eq. (66) and Eq. (67) temperature-dependent, with T_L as the lattice temperature.

The momentum and energy relaxation times for ODP are (8)

$$\begin{aligned}\frac{1}{\tau(\boldsymbol{p})} &= \frac{1}{\tau_m(\boldsymbol{p})} \\ &= \frac{\pi D_0^2}{2\rho\omega_o\Omega}(N_{\omega_o} + \tfrac{1}{2} \pm \tfrac{1}{2}) g_c(E \mp \hbar\omega_o)\end{aligned} \tag{69}$$

and

$$\frac{1}{\tau_E(\boldsymbol{p})} = \frac{1}{\tau(\boldsymbol{p})}\frac{\hbar\omega_o}{E(\boldsymbol{p})} \tag{70}$$

where g_c is the effective-mass density of states and is given by

$$g_c(E) = \frac{(2m^*)^{3/2}}{2\pi^2\hbar^3}\sqrt{E(\boldsymbol{p})} \tag{71}$$

We now turn our attention to the polar optical phonons (*POP*) which are the strongest scatterers in compound semiconductors such as GaAs. The scattering potential U_{POP} is given as [similar to Eq. (65)]

$$U_{pop}(\boldsymbol{x}, t) = \frac{q q^* u}{i\beta\Omega\epsilon_0} \tag{72}$$

where

$$\frac{q^{*2}}{\Omega} = \epsilon_0 \rho \frac{\omega_0^2}{k_0}\left(\frac{\kappa_0}{\kappa_\infty} - 1\right) \tag{73}$$

where k_0 and k_∞ are low and high frequency dielectric constants, respectively. The scattering integral yields

$$\begin{aligned} S(\boldsymbol{p}, \boldsymbol{p}') &= \frac{\pi q^2 \omega_0}{\kappa_0 \epsilon_0 \beta^2 \Omega}\left(\frac{\kappa_0}{\kappa_\infty} - 1\right)(N_{\omega_o} + \tfrac{1}{2} \pm \tfrac{1}{2}) \\ &\times \delta(\boldsymbol{p} - \boldsymbol{p} \mp \hbar\boldsymbol{\beta})\delta(E' - E \mp \hbar\omega_0)\end{aligned} \tag{74}$$

Schematic plots of scattering rates for acoustic phonons and optical phonons are shown, as functions of carrier energies, in Figs. 15 and 16, respectively. For more details and derivation of rate of other scattering sources as well as relaxation times see Ref. 8.

MOBILITY AND CONDUCTIVITY

By now we have seen the complexity of carrier dynamics in crystals. Electrons, while being accelerated by the applied electric field, interact with one or more scatterers, with results depending on the energy and momentum of the electrons. In spite of these impeding collisions, carriers do gain a net velocity from the applied electric field, which gives rise to conduction within the crystal. The complications in developing the theory of conduction by crystals are mainly because (9):

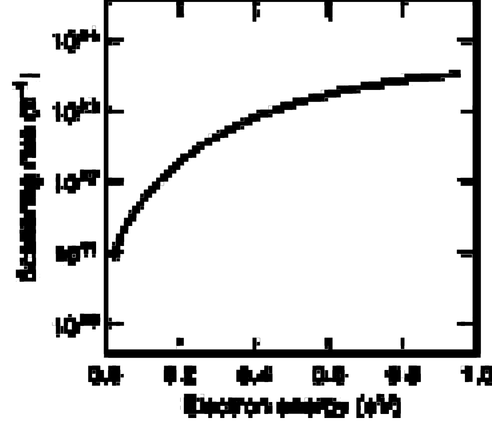

Figure 15. A schematic plot of acoustic phonon scattering rate versus electron energy for silicon at room temperature.

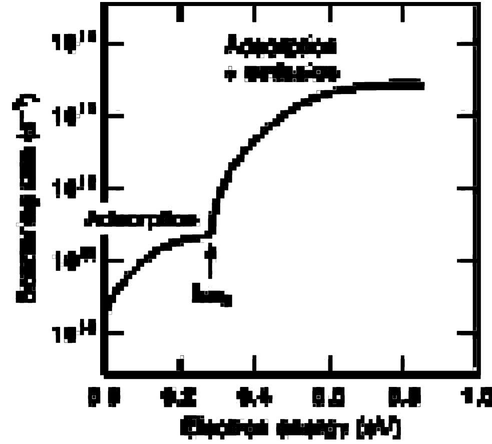

Figure 16. A schematic plot of optical phonon scattering rate versus electron energy for silicon at room temperature.

1. There are many scatterers, and the scattering rates are energy- as well as momentum-dependent.
2. More than one electron (and one phonon) participate in any appreciable conduction, and one must calculate the statistics of electron transport parameters.
3. The band structure [$E(\boldsymbol{k})$ relationship] of the semiconductor must be incorporated in the conduction model, because it relates the carriers' energy and momentum.

These complications can be circumvented by making a number of simplifying assumptions, most of which are rather well justified under low applied field. Here we follow Drude's (9) conduction model. First we assume that all electrons move with the same average velocity $\boldsymbol{v}$, given by

$$\begin{aligned}\hbar\boldsymbol{k} &= m\boldsymbol{v} \\ &= \boldsymbol{F}_0\end{aligned} \tag{75}$$

where $\boldsymbol{F}_0$ is the applied force. Second, we assign the effective mass m^* (discussed above) to incorporate the effects of

band structure of the semiconductor:

$$\begin{aligned}\hbar \dot{\boldsymbol{k}} &= m^* \dot{\boldsymbol{v}} \\ &= \boldsymbol{F}_0\end{aligned} \tag{76}$$

If there is no opposing force to $\boldsymbol{F}_0$, Eq. (76) leads to a continuous acceleration. Drude's model suggests that the effect of the scatterers is that of a friction force $\boldsymbol{F}_f$:

$$\boldsymbol{F}_f = \frac{m^* \boldsymbol{v}}{\tau} \tag{77}$$

where τ is the relaxation time associated with the dominant scattering effect. The equation of motion of electrons in the crystal then becomes

$$m^* \dot{\boldsymbol{v}} = \boldsymbol{F}_0 - \frac{m^* \boldsymbol{v}}{\tau} \tag{78}$$

Setting $\boldsymbol{F}_0$ equal to zero, for a moment, results in

$$m^* \dot{\boldsymbol{v}} = -\frac{m^* \boldsymbol{v}}{\tau} \tag{79}$$

which has a simple exponentially decaying solution of the form

$$\boldsymbol{v} \propto e^{-t/\tau} \tag{80}$$

making τ, the relaxation time, also the time constant with which the velocity of carriers decay to zero. With the applied field $\boldsymbol{E}$, the equation of motion becomes

$$m^* \dot{\boldsymbol{v}} = q\boldsymbol{E} - \frac{m^* \boldsymbol{v}}{\tau} \tag{81}$$

The steady-state solution of Eq. (81), when $\dot{\boldsymbol{v}} = \boldsymbol{0}$, is

$$\boldsymbol{v} = \frac{q\tau}{m^*}\boldsymbol{E} \tag{82}$$

But using $\boldsymbol{v} = \mu \boldsymbol{E}$ introduces the mobility μ of electrons as

$$\mu = \frac{q\tau}{m^*} \tag{83}$$

Equation (83) is indeed the definition of mobility. In arriving at this definition, we have assumed an average velocity for all electrons. Under low electric fields, the electron velocity is linearly proportional to the electric field:

$$\boldsymbol{v} = \mu \boldsymbol{E} \tag{84}$$

The electron current density is

$$\boldsymbol{J} = -qn\boldsymbol{v} \tag{85}$$

Therefore, for low fields,

$$\boldsymbol{J} = qn\mu \boldsymbol{E} \tag{86}$$

From the local form of Ohm's law,

$$\boldsymbol{J} = \sigma \boldsymbol{E} \tag{87}$$

where σ is the conductivity, we conclude

$$\sigma = qn\mu \tag{88}$$

The conductivity of crystals is significantly more complicated than the linear scalar coefficient given by Eq. (88). Specifically, when the conduction band structure (the spherical or ellipsoidal constant-energy surfaces) of the semiconductor is taken into consideration, the conduction process becomes much more complex. In the article entitled, we reexamine this simple model. In particular, we define a probability function $f = f(\boldsymbol{r}, \boldsymbol{p}, t)$ (a function of three variables: position $\boldsymbol{r}$, momentum $\boldsymbol{p}$, and time t, which constitute what is referred to phase space). Using this probability function, we then reexamine the process of averaging the carrier velocity. We also discuss multiscattering mobility.

TRANSPORT IN NANO-STRUCTURES

In recent years, the chip-making industry has been able to continually scale down the dimensions of the semiconductor devices used in CPU and DSP chips. While 0.18 μm and 0.13 μm are now yesterday's news in chip making, Intel is presently working on development of 40-nanometer chips with an anticipated marketing scheduled in the next five years. The wireless communication chip making has had a similar trend. The leap from 40 nanometers to less than 10 nanometers is expected in the next few years. In this Section we introduce several phenomena such as quantum well, quantum wire, and quantum dot that are encountered in nano-scale devices. These concepts are necessary for understanding the electronic transport in mesoscopic systems.

Mesoscopic Dimensions

The validity of the transport models described in the above Sections of this article become seriously questionable when the dimensions of the device are reduced below the mesoscopic threshold. Mesoscopic devices are structures that are small compared to the macroscopic scale, but large compared to the microscopic atomic scale. In order to determine whether the dimensions of a device are macroscopic or mesoscopic one needs to compare the device dimensions to one or more of the following characteristic lengths: (1) mean free path, which is the distance carriers move before their initial momentum is destroyed, (2) the De Broglie wavelength which is related to the kinetic energy of the carriers, and (3) the phase-relaxation length which is the distance carriers travel before their initial phase is destroyed (17). These characteristics lengths vary rather widely in different semiconductor materials with different doping levels and under different applied biases and operating temperatures. For this reason, the dimensions of the mesoscopic system can vary from a few nanometers to several micrometers. Considering all the limiting factors, the macroscopic transport models are valid in devices with gate lengths of up to about 30 nanometers (18), below which one needs to incorporate the mesoscopic transport phenomena.

Quantum Wells

With recent advances in nanoscale lithography techniques, a variety of nano-structures has been developed. In most of these structures, carriers (usually electrons) are confined in a narrow potential well, which can be created by forming a junction between two materials with different bandgaps. The simplest example of such system is the quantum well

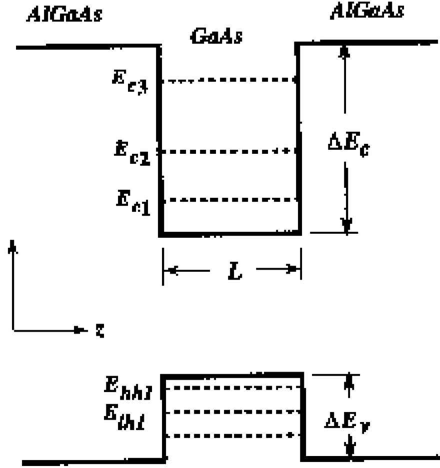

Figure 17. Type I $Al_xGa_{1-x}As/GaAs/Al_xGa_{1-x}As$ quantum well. After Ferry and Goodnick (18); reprinted with permission.

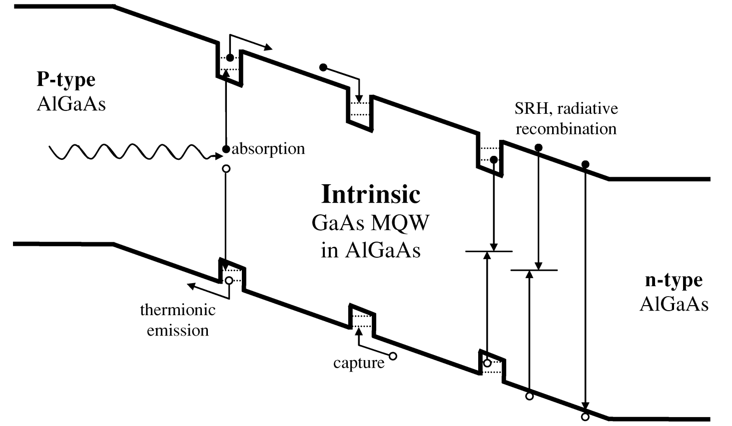

Figure 18. The energy band diagram of an $Al_xGa_{1-x}As/GaAs/Al_xGa_{1-x}As$ multiple quantum well (MQW) structures. Three quantum wells are embedded in the intrinsic GaAs region sandwiched between a p- $Al_xGa_{1-x}As$ region and an n-$Al_xGa_{1-x}As$ region. Several processes such as absorption of light, capture and escape of electrons and holes and radiative and non-radiative recombinations are depicted. After Ramey and Khoie (19); reprinted with permission.

formed by a thin layer of GaAs sandwiched between two layers of Al_x $Ga_{1-x}As$. The quantum well in the GaAs layer is the direct result of the difference in the bandgap of $Al_xGa_{1-x}As$ (with mole fraction of aluminum x between 0.1 and 0.45) and that of GaAs. The bandgap of $Al_xGa_{1-x}As$ at room temperature varies with x as Eg=1.424+1.245x for x<0.45 (18). For example with x=0.3, there is 375 meV difference between the bandgap of $Al_{0.3}Ga_{0.7}As$ and that of GaAs. This difference in badgap is split between the conduction band (65%) and valence band (35%) in the form of band discontinuity in the GaAs quantum well. Therefore, the depth of the quantum well in the conduction band (the discontinuity in the conduction band, that is) of GaAs is 243 meV while that of the valence band is 132 meV. The resulting quantum well is referred to as Type I and is shown in Figure 17. As the width (or length L) of the well is reduced, the quantization of energy levels in the well (for both electrons and holes) becomes more pronounced. In the quantum well shown in Figure 17, there are three bound states for electrons and three bound states for holes which include states for heavy holes, E_{hh}, and light holes, E_{lh}. Such quantum wells have been used in a variety of devices including high electron mobility transistors, resonant tunneling transistors, and multiple quantum well solar cells.

Modeling of the transport of carriers in structures with one or more embedded quantum wells (see Figure 18) requires knowledge of the quantized energy states (referred to as eigenstates) as well as the wavefuctions (referred to as eigenfunctions) of the carriers in the quantum wells. These eigenfunctions and eigenenergies are obtained from a field-dependent Schrödinger equation given by (19):

$$\left[\frac{\hbar^2}{2}\frac{d}{dx}\frac{1}{m^*(x)}\frac{d}{dx}+V(x)\right]\psi_i(x)=E_i\psi_i(x) \tag{89}$$

where E_i and ψ_i (x) are the energy level and the wavefunction of the subband i, respectively, and $V(x)$ is the potential profile in the device. A non-constant effective mass, $m^*(x)$, is used to account for different material systems throughout the $Al_xGa_{1-x}As$ regions and and the GaAs quantum wells.

The Schrödinger equation is solved together with Poisson equation:

$$\frac{\partial^2 V}{\partial x^2}=\frac{q}{\varepsilon}\left[N_A^- - N_D^+ + n_b + n_{qw} - p_b - p_{qw}\right] \tag{90}$$

The terms n_b and p_b are the bulk electron and hole densities, respectively, n_{qw} and p_{qw} are the quantum well electron and hole densities. N_D^+ and N_A^- are the ionized donor and acceptor doping levels, and ε is the dielectric constant.

In the presence of an electric field, the eigenenergies shift to higher energies as depicted in Fig. 19, where the eigenenergies and eigenfunctions are plotted versus position in a 100 Åquantum well. The eigenenergies are referenced to the bottom of the well, which is the corner of the well located at 160 Å. This shift is expected since a narrower well has its first eigenenergy higher than a wider well. The applied field causes the well to slant to a triangular bottom shape and thus acts as a narrower well. In certain situations, such as the system depicted in Fig 19, this increase in energy level can cause the highest level to become unbounded, which would then no longer contribute to the quantum well dynamics.

Quantum Wires

The movement of electrons that are confined in a quantum well is restricted in the direction perpendicular to the barriers, although thermal tunneling may aid their escape from the quantum well. This situation results in formation of a two-dimensional electron gas (2DEG), in which the electrons behave as two-dimensional entities. Further reduction in the dimensionality of electrons is possible by confining the 2DEG in another direction, which results in formation of a one-dimensional electron gas (1DEG). This can simply be realized by first forming a 2DEG, and then removing (etching) a portion of the material in which the

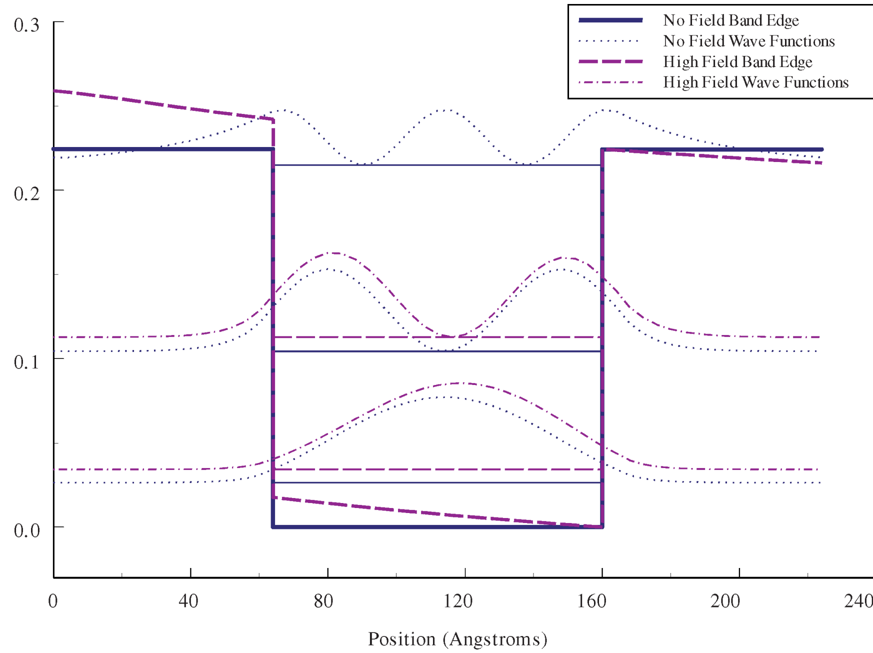

Figure 19. The eigenenergies and eigenfunctions of a GaAs quantum well in $Al_{0.3}Ga_{0.7}As$/GaAs system illustrating the effect of the applied field. Notice that in the presence of the electric field, the n = 3 eigenstate becomes unbounded. After Ramey and Khoie (19); reprinted with permission.

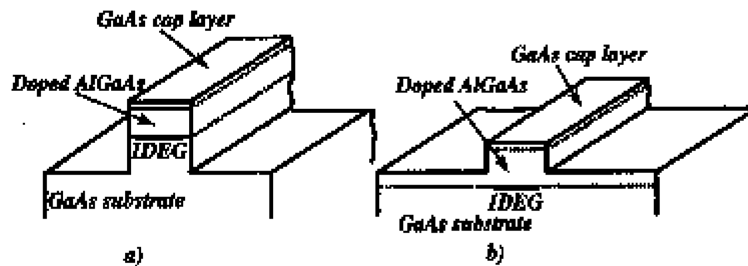

Figure 20. Realizations of quantum wire structures by etching quantum wells. In (a) the layers are etched below the 2DEG whereas in (b) the layers are partially etched. After Ferry and Goodnick (18); reprinted with permission.

2DEG has formed. The resulting structure is called a quantum wire. Two different realizations of quantum wire structures are shown in Fig. 20.

Quantum Dots

The degree of freedom of carriers in a quantum wire can further be reduced to zero-dimension (0DEG) by removing the material in the remaining direction. The resulting structure is referred to as a quantum dot (or quantum box). Figure 21(a) shows an idealized quantum dot coupled to two external leads through which the dot is connected to an external circuit. This structure is called a Coulomb island, and can be realized by depositing clusters of metal (gold) in a dielectric medium such as aluminum oxide as shown in Figure 21(b).

The mechanism for transferring electrons to and from the Coulomb island is quantum tunneling. The energy required for charging of the dot with just one electron is:

$$E(charging) = \frac{1}{2}\frac{e^2}{C} \tag{91}$$

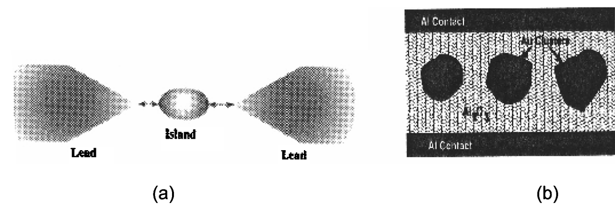

Figure 21. (a) An idealized Coulomb island, and (b) realization of a Coulomb island using metal clusters on an insulator. After Ferry and Goodnick (18); reprinted with permission.

Where E is the energy required to charge the island, ε is the charge of electron (1.602×10^{-19} Coulomb), and C is the capacitance of the island. The average thermal energy of electrons is:

$$E(thermal) = k_B T \tag{92}$$

Equating the energy required to charge the island with that of the average thermal energy results in the largest value of the capacitance $C = 0.003$ femto Farad. Calculation shows that for this largest capacitance, the largest size the

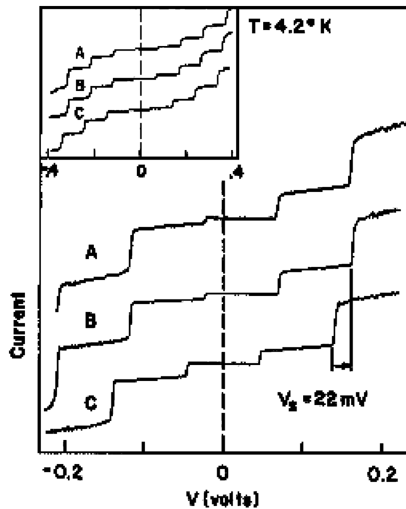

Figure 22. Experimental (A) and theoretical (B and C) I-V characteristics from an STM-contacted 10 nm diameter In droplet showing the Coulomb staircase. After Ferry and Goodnick (18); Originally after Wilkins, et. al (20); reprinted with permission.

island can have is 30 nanometers. (See Ferry and Goodnick (18).) In other words, with an island smaller than about 30 nm, addition of even one single electron can alter the potential of the island drastically and lead to a phenomenon called Coulomb blockade in which the tunneling of electrons is blocked until the required charging energy is provided by increase in the applied bias. The resulting I-V characteristics of such Coulomb island resembles a staircase (referred to as Coulomb staircase) and is shown in Figure 22.

BIBLIOGRAPHY

1. P. Y. Yu M. Cardona *Fundamentals of Semiconductors*, New York: Springer-Verlag, 1996.
2. R. L. White *Basic Quantum Mechanics*, New York: McGraw-Hill, 1966.
3. A. Yariv *An Introduction to Theory and Applications of Quantum Mechanics*, New York: Wiley, 1982.
4. D. K. Ferry *Semiconductors*, New York: Macmillan, 1991.
5. S. Datta *Quantum Phenomena*, Modular Series on Solid State Devices VIII, Reading, MA: Addison-Wesley, 1989.
6. R. F. Pierret *Advanced Semiconductor Fundamentals*, Modular Series on Solid State Devices VI, Reading, MA: Addison-Wesley, 1987.
7. S. Wang *Fundamentals of Semiconductor Theory and Device Physics*, Englewood Cliffs, NJ: Prentice-Hall, 1989.
8. M. Lundstrom *Fundamentals of Carrier Transport*, Modular Series on Solid State Devices X, Reading, MA: Addison-Wesley, 1990.
9. K. Hess *Advanced Theory of Semiconductor Devices*, Englewood Cliffs, NJ: Prentice-Hall, 1988.
10. J. S. Blakemore Semiconducting and other major properties of gallium arsenide, *J. Appl. Phys.*, **53**: R123–R181, 1982.
11. S. M. Sze *Physics of Semiconductor Devices*, 2nd ed., New York: Wiley, 1981.
12. J. M. Ziman *Electron and Phonons, The Theory of Transport Phenomena in Solids*, London: Oxford Univ. Press, 1960.
13. J. P. McKelvey *Solid State and Semiconductor Physics*, New York: Harper and Row, 1966.
14. J. L. T. Waugh G. Dolling *Phys. Rev.*, **132**, 2410, 1963.
15. W. A. Harrison *Solid State Theory*, New York: Dover, 1980.
16. B. R. Nag *Electron Transport in Compound Semiconductors*, New York: Springer-Verlag, 1980.
17. S. Datta, *Electronic Transport in Mesoscopic System*, Cambridge, United Kingdom, Cambridge University Press, 1995.
18. D. K. Ferry and S. Goodnick, *Transport in Nanostructures*, Cambridge, United Kingdom, Cambridge University Press, 1997.
19. S. Ramey and R. Khoie,“ Modeling of Multiple Quantum Well Solar Cells Including Capture, Escape, and Recombination of Photo-excited Carriers in Quantum Wells,” *IEEE Transactions on Electron Devices*, **50**, 1179–1188, 2003.
20. R. Wilkins, E. Ben-Jacob, and R. C. Jaklevic, *Physical Review Letters*, **63**, 801, 1989.

R. KHOIE
R. VENKAT
University of the Pacific, Stockton, CA
University of Nevada, Las Vegas, Las Vegas, NV